J Therm Anal Calorim (2010) 101:81–88
DOI 10.1007/s10973-010-0713-0

Thermal analysis of the ω nanophase transformation from the metastable β Ti–12Mo alloy

Fan Sun · Denis Laillé · Thierry Gloriant

Received: 12 June 2009 / Accepted: 9 February 2010 / Published online: 11 March 2010

Abstract In this study, the thermal analysis of the ω nanophase transformation from a quenched metastable β Ti–12Mo alloy composition (mass%) was investigated by electrical resistivity and dilatometry measurements. The activation energy was observed to be 121 ± 20 kJ mol^{-1} (from resistivity measurements) and 114 ± 12 kJ mol^{-1} (from dilatometry measurements) during the early stage of the transformation process. The kinetic of the ω nanophase transformation was modelized by using the classical Johnson–Mehl–Avrami (JMA) theory and a modified Avrami (MA) analysis. An Avrami exponent close to 1.5 was found at the early stage of the transformation suggesting a pure growth mechanism from pre-existing nucleation sites. Nevertheless, it was observed a decrease of the Avrami exponent to 0.5 at higher transformed fraction demonstrating a dimension loss in the growth mechanism due to the existence of the high misfit strain at the interface β/ω.

Keywords Titanium alloy · Dilatometry · Electrical resistivity · Activation energy · Kinetic

Introduction

Over the last few decades, the interest of titanium alloys has become more and more important in many application fields (aeronautic, biomedical, chemistry, etc.) because of their properties of high strength, excellent hardenability, low density and good corrosion resistance [1]. In titanium-based alloys, it has been reported a possible nanostructuration leading to a general improvement of the mechanical properties and a considerable strengthening. This nanostructuration is due to the precipitation of the nanoscale ω phase (20–30 nm in size), which is observed in metastable β Ti-based alloys (quenching from the β phase field) containing appropriate β-stabilizer elements such as Fe, Mo, Ta, Nb, Cr and/or V [2–7].

It has been reported that the ω nanophase transition could be particularly well detected on heating by means of the electrical resistivity and dilatometry measurement techniques. These methods are well known to be very sensitive to minor constitutional changes produced by quenching, ageing and precipitation treatments [8–13]. In this study, a binary metastable β Ti–Mo alloy containing 12 mass% of molybdenum element was synthesized and then characterized by employing electrical thermo-resistivity and thermo-dilatometry measurements. The nanoscale ω phase transformation process in Ti–12Mo alloy was investigated under different isothermal conditions by applying the classical Johnson–Mehl–Avrami (JMA) theory and a modified Avrami (MA) plot method. With this combined approach, Avrami exponents and activation energies were determined in order to clarify the ω nanophase transformation kinetic process from the metastable β state with the objective to develop a new generation of high-strength nanostructured Ti-based alloys.

Experimental

The binary Ti–12Mo (mass%) alloy was synthesized by the cold crucible levitation melting (CCLM) technique in an induction furnace (CELES high frequency generator). The melting was carried out under a pure Ar atmosphere after

F. Sun · D. Laillé · T. Gloriant (✉)
INSA Rennes, UMR CNRS 6226 Sciences Chimiques de Rennes/Chimie-Métallurgie, 20 avenue des Buttes de Coësmes, Rennes 35043, France
e-mail: Thierry.Gloriant@insa-rennes.fr

several cycles of high vacuum pumping. Notable features of CCLM are that it can melt metals with a high melting point, create an alloy of uniform composition and prevent the crucible contamination [14]. The obtained ingots (weight of about 20 g) were remelted in a laboratory scale arc furnace (7400 TÜBINGEN, Edmund Bűhler), under pure argon atmosphere. Near cylindrical ingots with a diameter of about 10 mm and a length of about 25 mm were obtained. The ingots were then solution treated in the β-phase domain at 1,223 K under high vacuum (10^{-6} mbar) for 2 h in a tubular furnace and then quenched in water at room temperature to obtain the metastable β microstructure. Specimens of two different shapes for electrical resistivity measurements and dilatometry measurements, respectively, were cut from the ingots and cleaned in an acidic bath (10% HF in nitric acid HNO_3).

The resistivity measurements were performed by using the four-probe method with a serial electrical circuit set-up composed of: the sample (cut into a thin 20 mm × 2 mm × 0.7 mm lamella in contact with the thermocouple for measuring the temperature), a reference resistor R_{ref} (2 Ω), a d.c. source and a computer-controlled data acquisition system (self-designed apparatus). All the experiments were carried out under high vacuum (10^{-6} mbar) from room temperature. In order to suppress the parasites, the sample was placed in the middle of a molybdenum tube as a Faraday cage during the measurement. In non-isothermal conditions, a constant heating rate of 2 K min^{-1} was used and for the isothermal measurements, the desired temperatures (421, 431, 441 and 451 K) were reached at 2 K min^{-1} after holding the sample at 363 K for 2 h to eliminate the thermal stress. For the dilatometry measurements (self-designed apparatus), all the samples were cut into a square rod (dimension: 18 mm × 4.2 mm × 4.2 mm). The dilatometry variation, ΔL, of the sample, in contact with the thermocouple for measuring the temperature, was carried out under high vacuum (10^{-6}–10^{-7} mbar). In non-isothermal conditions, a constant heating rate of 2 K min^{-1} was used and for the isothermal measurements, the desired temperatures (421, 431 and 441 K) were reached at 2 K min^{-1} after holding the sample at 363 K for 2 h. In order to determine the transformed fraction by dilatometry, the maximum variation, ΔL_{max}, was measured to be 12.7 μm by an isothermal treatment at 441 K until no length change happened.

Results and discussion

Non-isothermal measurements

The non-isothermal characterizations of the transformation process from the Ti–12Mo quenched alloy were performed by relative electrical resistivity and dilatometry measurements under continuous heating conditions. Figure 1 shows the resistivity and the dilatometry variation curves from 363 K to about 1,200 K (heating rate: 2 K min^{-1}). In this figure, the derivative of the dilatometry signal is also indicated in dash line. The transformation sequence from the metastable β state carried out on different Ti-based alloys has been recently established by our group and the curves obtained in the present study are in accordance with our previous observations [10, 13]. Thus, it has already been reported that the negative temperature dependence (NTD) observed on the resistivity curve at low temperature ($T < 450$ K) is due to the presence of the athermal ω phase (ω_{ath}), which is formed during quenching [3, 10, 15]. At higher temperature, the hexagonal isothermal ω nanophase (ω_{iso}) was observed to precipitate implying diffusional phenomenon. With the Ti–12Mo alloy, the formation of this ω_{iso} phase on heating is shown to occur at about 451 K (identified by $T\omega_{iso}$ in Fig. 1), where an increase of the resistivity and a decrease of the dilatometry are observed simultaneously. From about 611 K, the resistivity drop and the dilatometry rate change observed (indicated by $T\alpha_{nano}$ in Fig. 1) are due to the progressive vanishing of ω_{iso} phase through a ω/α-phase transformation. By heating the alloys at a higher temperature, the precipitation of a conventional intergranular and intragranular α phase occurs at about 836 K, where a sudden change in both resistivity and dilatometry curves are observed ($T\alpha_{eq}$ in Fig. 1).

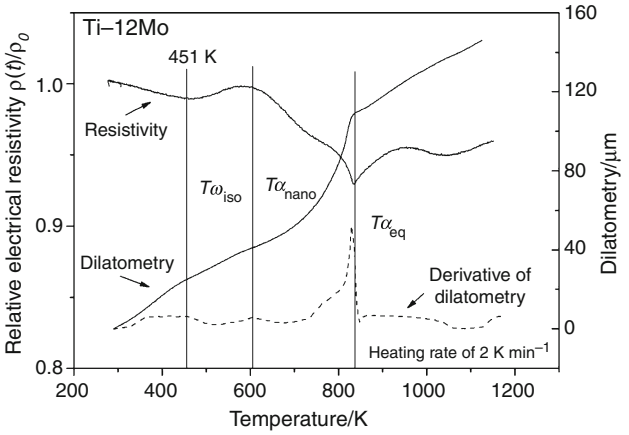

Fig. 1 Non-isothermal scans obtained from the as-quenched Ti–12Mo alloy by relative electrical resistivity and dilatometry measurements (heating rate: 2 K min^{-1})

Isothermal measurements

Four isothermal temperatures (421, 431, 441 and 451 K) by resistivity and three (421, 431 and 441 K) by dilatometry were chosen to characterize the ω_{iso} nanophase formation. Figure 2 presents the curves obtained for the different

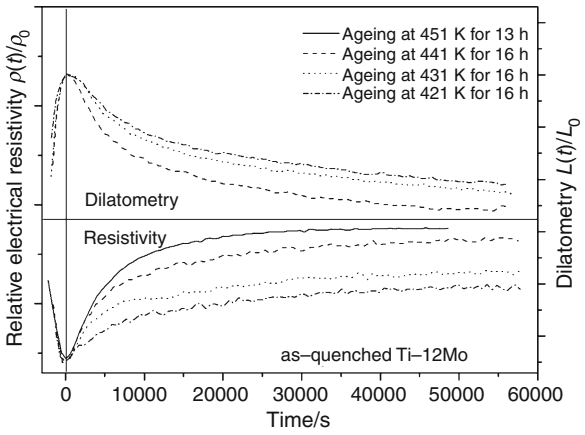

Fig. 2 Isothermal curves of the ω_{iso} transformation process from resistivity (421, 431, 441 and 451 K) and from dilatometry (421, 431 and 441 K) measurements

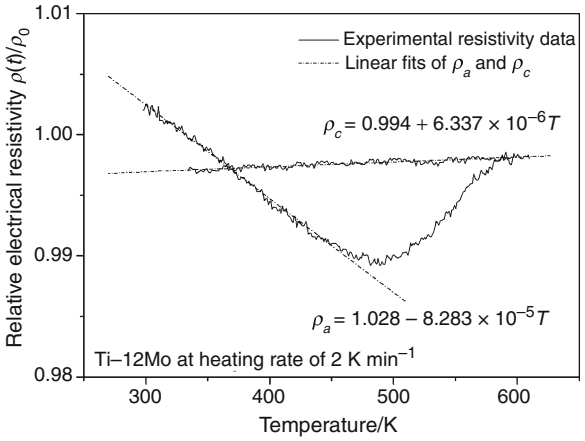

Fig. 3 Electrical resistivity variation from the as-quenched Ti–12Mo alloy under non-isothermal heating to 611 K at 2 K min^{-1} and spontaneously cooling. The *dash lines* refer to linear fitting of Eqs. 2 and 3, respectively

isothermal treatments by electrical resistivity and by dilatometry, respectively. On theses curves, the time was initialized precisely when the desired temperature was reached. In this study, the traditional JMA theory was applied to characterize the nucleation and growth mechanism. From the JMA theory, the overlapping and impingements between the extended volumes are taken into account and the transformed fraction, α, detected by resistivity and by dilatometry measurements can be simply written as [16–19]:

$$\frac{d\alpha}{d\alpha_{ext}} = 1 - \alpha \tag{1}$$

where α is the detected transformed fraction of the ω_{iso} transformation and α_{ext} volume fraction of the extended volumes of ω_{iso}. α_{ext} can be described as $\alpha_{ext} = V_{ext}/V_0$ where V_0 is the total transformed volume.

In order to determine the kinetic parameters related to the ω_{iso} phase transformation, electrical resistivity and dilatometry models are needed to evaluate the transformed fraction, α. From the electrical resistivity measurements, the 3D resistivity model proposed by Landauer [20] was applied to analyze the transformed fraction during the ω_{iso} phase precipitation. For that, the temperature variation of the relative resistivity normalized to room temperature value was approximated from the non-isothermal measurements as shown in the Fig. 3 with:

$$\rho_a = 1.028 - 8.283 \times 10^{-5} T \tag{2}$$

for the as-quenched metastable β state and

$$\rho_c = 0.994 + 6.337 \times 10^{-6} T \tag{3}$$

at the end of ω_{iso} transformation.

In this model, it is assumed that 3D spherical regions of one phase are surrounded by a uniform matrix, and consequently, the transformed fraction can be evaluated by the resistivity measurements as follow:

$$\rho_m(\alpha, t) = -\frac{1}{2}\left[(2-3\alpha)\rho_c + (3\alpha-1)\rho_a - \sqrt{[(2-3\alpha)\rho_c + (3\alpha-1)\rho_a]^2 + 8\rho_a\rho_c}\right] \tag{4}$$

where α is the ω_{iso} transformed fraction and ρ_a and ρ_c are given by Eqs. 2 and 3, respectively.

From the dilatometry measurements, the volume change of the sample is assumed to be isotropic, and the model can be simply described as [21]:

$$\alpha(t) = \frac{L(t) - L_0}{L_f - L_0} = \frac{\Delta L(t)}{\Delta L_{max}} \tag{5}$$

where L_0 is the initial length, L_f final length at the end of the complete transformation and α represents the ω_{iso} transformed fraction.

By applying Eqs. 4 and 5 to the experimental data obtained by resistivity and by dilatometry, respectively, the different curves of ω_{iso} phase transformed fraction, α, vs. isothermal annealing time, t, can be established and are presented in Fig. 4. In this figure, the curves obtained from both methods at the same isothermal temperature seem to be identical but a noticeable distinction between resistivity (Fig. 4a) and dilatometry (Fig. 4b) measurements can be found at the very beginning of the transformation process. Indeed, an incubation time delay, τ, is observed on the dilatometry results, which can lead experimentally to a large uncertainty of the kinetic parameters. According to our experimental data, this time delay is estimated to be around 300 s. Therefore, the classical JMA method and an

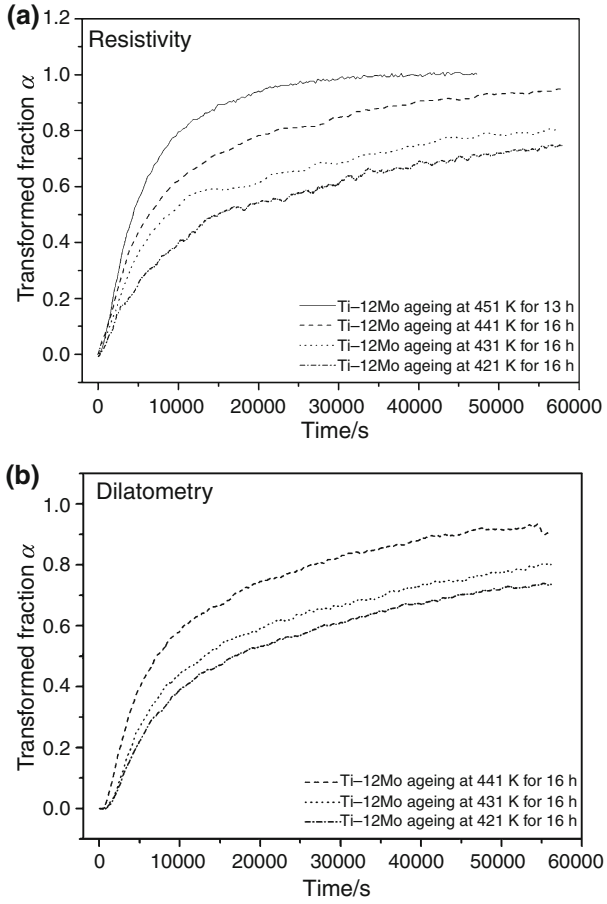

Fig. 4 Kinetic curves showing the ω_{iso} transformed fraction vs. time: **a** from isothermal resistivity measurements and **b** from isothermal dilatometry measurements

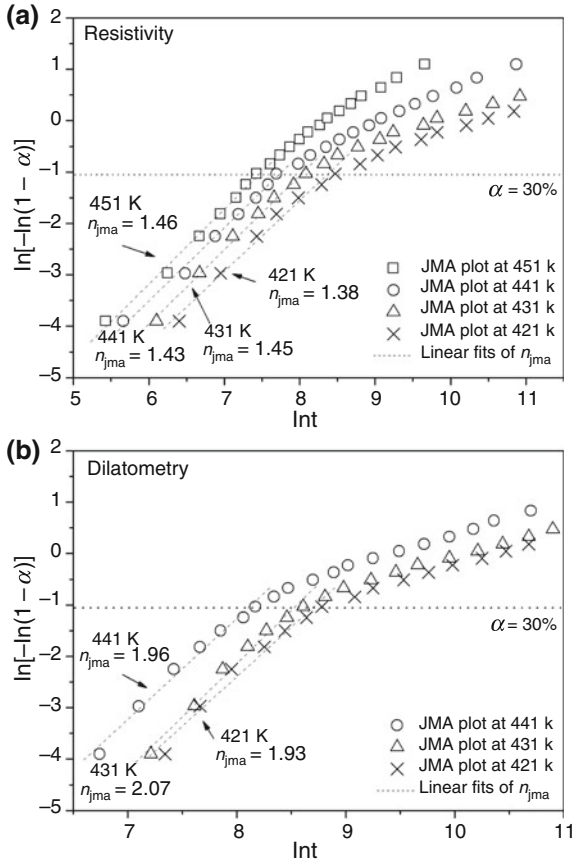

Fig. 5 Classic JMA plots of the Avrami exponents during the ω_{iso} transformation process: **a** from resistivity results shown in Fig. 4a and **b** from dilatometry results shown in Fig. 4b. The *dash lines* refer to linear fitting of the different plots

additional MA [22] plot were both applied to determine the transformation kinetic of the ω_{iso} phase from the as-quenched Ti–12Mo alloy.

The transformation kinetic of the ω_{iso} nanophase

The Johnson–Mehl–Avrami method

The JMA equation (6), deduced from Eq. 1, is successfully used in describing the transformation kinetics in alloys under isothermal conditions:

$$\alpha(t) = 1 - \exp(-Kt^n) \tag{6}$$

with

$$K(T) = k_0 e^{-E_a/\mathrm{RT}} \tag{7}$$

where n is the Avrami exponent (indicative of the transformation process) and K is a thermally activated rate constant representing both nucleation and growth rates, which can be described by an Arrhenius relation, in which E_a is the apparent activation energy.

Over the full range of the ω_{iso} transformation, the experimental Avrami exponent, n_{JMA}, can be determined from both resistivity and dilatometry results by using the JMA plot (8) as proposed in literature [23–25] :

$$\ln[-\ln(1-\alpha)] = n_{JMA} \ln t + \ln K \tag{8}$$

The calculation of n_{JMA} is then evaluated by plotting ln $[-\ln(1-\alpha)]$ vs. ln$t$ and the results obtained with an α increment of 5% (to minimize the noises from experiments) from all electrical resistivity and dilatometry curves are shown in Fig. 5.

In this figure, it is observed, from resistivity (Fig. 5a) and dilatometry (Fig. 5b) measurements, an appreciable deviation from the linearity through the whole ω_{iso} transformation. This deviation indicates a change of the nucleation and growth mechanism during the transformation and the JMA theory can only be valid at the early stage of the transformation process ($\alpha < 30\%$) in the present case. On the other hand, a significant difference of the measured n_{JMA} parameter obtained by both methods is also observed when the transformed fraction is <30%. From the

resistivity results (Fig. 5a), an Avrami exponent was determined at about 1.5, which indicates a pure growth mechanism from pre-existing nuclei sites. On the contrary, an Avrami exponent close to 2 was evaluated for the three isothermal temperatures by dilatometry (Fig. 5b) indicating a possible nucleation mechanism at the early stage of the ω_{iso} transformation [24]. The contradiction involved here is probably due to the large uncertainty associated with an effective time lag [25] that we observed from our experimental results. Therefore, the problem of time lag must be taken into account and a MA plot method was also used in this study.

The modified Avrami method

The effective time lag, τ, indicates that an incubation time is necessary for obtaining a critical-size nuclei population [24]. According to the non-steady theory of nucleation [26, 27], the observed experimental incubation time, τ, can be expressed as:

$$\tau = \tau_0 + \tau_\beta \tag{9}$$

where τ_0 is the time for the non-steady state nucleation and τ_β is the time required to attain an observable degree of transformation experimentally. With these considerations, the classic JMA equation (6) is often rewritten as:

$$\alpha(t) = 1 - \exp\{-K(t-\tau)^n\} \tag{10}$$

For the accurate determination of Avrami exponent, it has been proposed [22] an original and simple method called the MA plot, for which an exact knowledge of τ is not necessary. The detailed procedure consists of eliminating the explicit form $(t - \tau)$, which appears in Eq. 10, by substitution of the Arrhenius equation (7). Then the new fitting equation can be expressed as follow:

$$\ln[-\ln(1-\alpha)] = \frac{-1}{n-1}\ln(nK) + \frac{n}{n-1}\ln\left(\frac{d\alpha/dt}{1-\alpha}\right) \tag{11}$$

In the Fig. 6 are presented the results obtained by plotting ln $[-\ln(1 - \alpha)]$ vs. ln $[(d\alpha/dt)/(1 - \alpha)]$ from electrical resistivity and dilatometry measurements, respectively. The good accordance between the two graphs (Fig. 6a, b) indicates that the influence of the time lag was successfully taken into account with the MA method. Consequently, accurate n values can be obtained from this MA method. From these plots, experimental Avrami exponents, n_{MA}, and activation energy, E_a, can be easily deduced and the results are presented in Table 1. At the beginning of the ω_{iso} transformation, the Avrami exponents evaluated from electrical resistivity measurements and analyzed both by JMA and MA approaches are in the same order of magnitude at about 1.5. On the other hand, it is also obtained from dilatometry results an Avrami exponent close to 1.5 at the beginning of the transformation when the MA method is applied, which is in good accordance with the resistivity results this time. Consequently, a strong incubation time influence is observed by dilatometry probably due to the temperature gradient existing between the surface and the core of the bulk sample used for the measurements. Therefore, the MA method is much more recommended for the investigation of the phase transformation kinetic by dilatometry analysis.

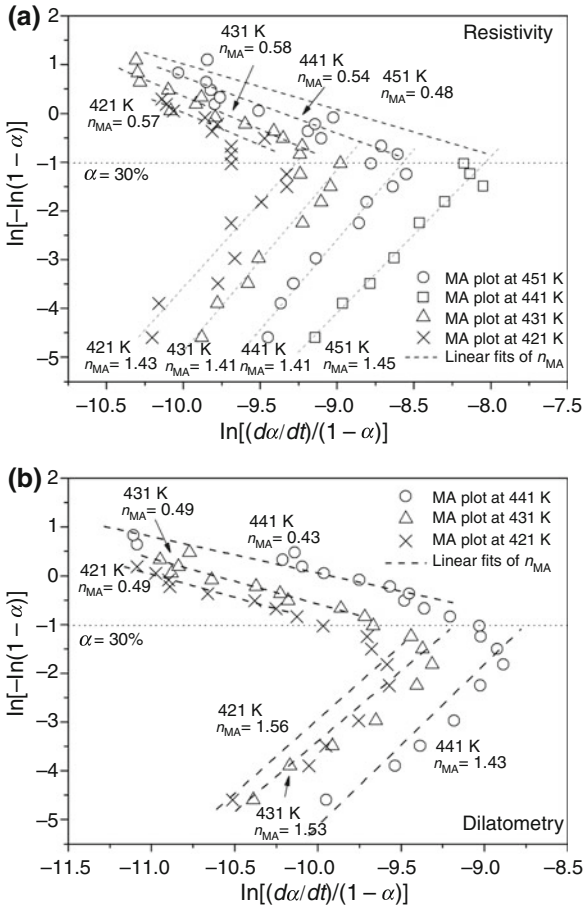

Fig. 6 Modified Avrami (MA) plots of the whole ω_{iso} transformation: **a** from resistivity results calculated from the kinetic curves shown in Fig. 4a and **b** from dilatometry results calculated from the kinetic curves shown in Fig. 4b. The *dash lines* refer to the linear fitting of the Avrami exponents

The ω_{iso} nanophase transformation mechanism

From the combined JMA and MA analysis, the value of the Avrami exponent, found close to 1.5, clearly indicates that the ω_{iso} nanophase formation is governed by a pure growth mechanism of spherical particles during the early stage of the transformation process. This pure growth mechanism illustrates that nucleation sites already exist in the β matrix, which is in good accordance with previous studies

Table 1 Kinetic parameters and activation energies results for the ω_{iso} nanophase transformation from electrical resistivity and dilatometry measurements for the different isothermal conditions

T/K	Transformation process				
	Early stage ($\alpha < 30\%$)				Later stage ($\alpha > 30\%$)
	$n_{JMA}(\pm 0.05)$	$n_{MA}(\pm 0.1)$	$K_T(\times 10^{-6})$	E_a (± 20 kJ mol^{-1})	n_{MA} (± 0.1)
Resistivity					
421	1.38	1.43	0.97	121 kJ mol^{-1}	0.57
431	1.45	1.41	1.23		0.58
441	1.43	1.41	2.47		0.54
451	1.46	1.45	10.18		0.48
T/K	Transformation process				
	Early stage ($\alpha < 30\%$)				Later stage ($\alpha > 30\%$)
	n_{JMA} (± 0.05)	n_{MA} (± 0.15)	K_T ($\times 10^{-6}$)	E_a (± 12 kJ mol^{-1})	n_{MA} (± 0.1)
Dilatometry					
421	1.93	1.56	0.98	114 kJ mol^{-1}	0.49
431	2.07	1.53	2.03		0.49

concerning the ω phase formation. As already mentioned, it is widely observed the presence of the athermal ω phase (ω_{ath}) in quenched metastable β-Ti-based alloys. A $(111)_\beta$ plane collapse model has been proposed to explain this displacive transformation: the ω_{ath} lattice can be obtained by collapsing one pair of (111) planes to the intermediate position leaving the adjacent (111) planes unaltered [28]. Thus, the presence of such phase in the as-quenched metastable β matrix represents a favourable source of nucleation sites for the growth of the ω_{iso} nanoparticles.

The significant change in linearity at higher transformed fraction ($\alpha > 30\%$), which was observed with the classical JMA plots (Fig. 5) is also detected on the MA plots presented in Fig. 6. This situation indicates the limitation in the use of the JMA theory as it is observed for many phase transformation kinetic studies like the nanocrystallization from amorphous alloys for example [29]. The diffusion field impingement between very close adjacent nanoparticles is widely considered to be the reason of this limitation but in the present case a different explanation can be considered. According to the TEM observations carried out on ω_{iso} [30, 31] in the Ti–Mo system, the morphology of this phase at the later stage of the transformation is observed ellipsoidal in shape rather than spherical as it is at the early stage. The dimensionality loss of the ω_{iso} nanoprecipitates occurring during the whole diffusion-controlled process is due to the existence of a high misfit strain at the interface ω_{iso}/β [3–7, 28]. This misfit, resulting to a mismatch between the two phases, leads to the preferential $<111>_\beta$ growth directions and an ellipsoidal shape morphology tendency is then observed in the Ti–Mo system. Taking into account the existence of a high misfit strain at the interface, a schematic representation of the ω_{iso} phase transformation from the as-quenched Ti–12Mo alloy during the whole process is presented in the Fig. 7. At the beginning of the transformation, ω_{iso} particles grow directly from pre-existing nucleation sites related to the quenched ω_{ath} nanophase particles (Fig. 7a). During this early stage, the ω_{iso} particle kinetic growth is governed by the diffusion of the Mo element rejected to the surrounding β matrix. As the dimension of the spherical particles is very small at this stage, the strain misfit at ω_{iso}/β interface (gray

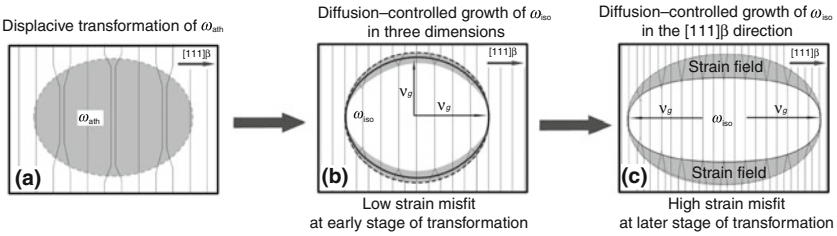

Fig. 7 Schematic representations of the ω_{iso} phase transformation sequence during the whole process

area in Fig. 7b) remains sufficiently weak and the diffusion mechanism is not altered. At the later stage of the transformation process, a high misfit strain volume (gray area in Fig. 7c) surrounding ω_{iso} particles severely drawback the growth rate except in $<111>_{\beta}$ direction. Therefore, a privileged diffusion growth dominates the rest of the process and leads to a ω_{iso} ellipsoidal shape morphology along the $<111>_{\beta}$ direction.

Conclusions

In this study, the thermal analysis by means of both electrical resistivity and dilatometry methods was found to be very useful to obtain experimental datas and to lead a theoretical modelling concerning the ω_{iso} nanophase precipitation from the metastable β Ti–12Mo alloy. By these methods, the activation energy, E_a, was measured to be 121 ± 20 kJ mol^{-1} (resistivity) and 114 ± 12 kJ mol^{-1} (dilatometry) during the early stage of transformation process. The classical JMA approach and a MA method, used in this study, were found to be efficient to analyze the ω_{iso} nucleation and growth mechanism only at low transformed fraction. An Avrami exponent close to 1.5 was found at the early stage of the transformation suggesting a pure growth mechanism from pre-existing nucleation sites related to the presence of quenched ω_{ath} nanophase in the β matrix. For a higher transformed fraction value (>30%), it was observed a decrease of the Avrami exponent to 0.5 demonstrating a dimension loss in the growth of the ω_{iso}. This change is attributed to the existence of the high misfit strain at the interface β/ω_{iso} in the Ti–Mo system, in which ellipsoidal shape morphology of the ω_{iso} nanoparticles is observed at the final stage of the transformation.

Acknowledgements This study was supported by China Scholarship Council (CSC) and INSA-Rennes (France) in the framework of UT-INSA project (2006–2009).

References

1. Eylon D. Issues in the development of beta titanium alloys. In: Proc 1 Int Symp Metall Technol Pract Titanium Alloys; 1994. p. 29.
2. Ankem S, Green CA. Recent developments in microstructure/property relationships of beta titanium alloys. Mater Sci Eng A. 1999;263:127–31.
3. Williams JC, Blackburn MJ. The influence of misfit on the morphology and stability of the omega phase in titanium-transition metal alloys. Trans Met Soc AIME. 1969;245:2352–5.
4. Yamane T, Miyakubi A. Omega phase formation in Ti–Fe alloys. Met Soc AIME. 1980;2:1309–16.
5. Krishman R, Naik UM. Omega and alpha precipitation in Ti–15Mo alloy. Met Soc AIME. 1980;2:1335.
6. Takemoto Y, Hida M, Sakakibara A. Mechanism of omega → alpha transformation in beta -titanium alloy. J Jpn Inst Met. 1993;57:261–7.
7. Duerig TW, Terlinde GT, Williams JC. Phase transformations and tensile properties of Ti-10 V–2Fe–3Al. Metall Trans A. 1980;11:1987–98.
8. Chung DDL. Thermal analysis by electrical resistivity measurement. J Therm Anal Calorim. 2001;65:153–65.
9. Morra PV, Bottger AJ, Mittemeijer EJ. Decomposition of iron-based martensite. A kinetic analysis by means of differential scanning calorimetry and dilatometry. J Therm Anal Calorim. 2001;64:905–14.
10. Gloriant T, Texier G, Prima F, Laillé D, Gordin DM, Thibon I, et al. Synthesis and phase transformations of beta metastable Ti-based alloys containing biocompatible Ta, Mo and Fe beta-stabilizer elements. Adv Eng Mater. 2006;8:961–5.
11. Hill MA, Polonis DH. Influence of beta phase decomposition on the temperature coefficient of resistivity of titanium alloys. J Mater Sci. 1987;22:2181–4.
12. Prima F, Vermaut P, Ansel D, Debuigne J. Omega precipitation in a beta metastable titanium alloy, a resistometric study. Mater Trans JIM. 2000;41:1092–7.
13. Gloriant T, Texier G, Sun F, Thibon I, Prima F, Soubeyroux JL. Characterization of nanophase precipitation in a metastable β titanium-based alloy by electrical resistivity, dilatometry and neutron diffraction. Scripta Mater. 2008;58:271–4.
14. Gordin DM, Delvat E, Chelariu R, Ungureanu G, Besse M, Laille D, et al. Characterization of Ti–Ta alloys synthesized by cold crucible levitation melting. Adv Eng Mater. 2008;10:714–9.
15. Ikeda M, Komatsu SY, Sugimoto T, Kamei K. Negative temperature dependence of electrical resistivity in Ti–Mo binary alloys. In: Proc Sixth World Conference on Titanium, les Editions de Physique, Paris; 1988. pp. 313–8.
16. Avrami M. Kinetics of phase change. I General theory. J Chem Phys. 1939;7:1103–12.
17. Avrami M. Kinetics of phase change. II Transformation-time relations for random distribution of nuclei. J Chem Phys. 1940;8:212–24.
18. Avrami M. Kinetics of phase change. III Granulation, phase change, and microstructure kinetics of phase change. J Chem Phys. 1941;9:177–84.
19. Johnson WA, Mehl RF. Reaction kinetics in processes of nucleation and growth. Trans Am Inst Min Metall Pet Eng. 1939;135:416.
20. Landauer R. The electrical resistance of binary metallic mixtures. J Appl Phys. 1952;23:779–84.
21. Van Bohemen SMC. Van der Laars M, Sietsma J, Van der Zwaag S. Modelling of the $\beta \rightarrow \alpha + \beta$ transformation in a metastable β Ti alloy based on the growth kinetics and the morphology of the α plates. Int J Mater Res. 2007;98:476–84.
22. Mao M, Altounian Z. Accurate determination of the Avrami exponent in phase transformations. Mater Sci Eng A. 1991;149:L5–8.
23. Calka A, Radlinski AP. Decoupled bulk and surface crystallization in $Pd_{85}Si_{15}$ glassy metallic alloys: description of isothermal crystallization by a local value of the Avrami exponent. J Mater Res. 1988;3:59–66.
24. Christian JW. The theory of transformation in metals and alloys, Part 1. Oxford: Pergamon Press; 1975.
25. Cumbrera FL, Sanchez-Bajo F. The use of the JMAYK kinetic equation for the analysis of solid-state reactions: critical considerations and recent interpretations. Thermochim Acta. 1995;266:315–30.
26. Ghosh G, Chandrasekaran M, Delaey L. Isothermal crystallization kinetics of $Ni_{24}Zr_{76}$ and $Ni_{24}(Zr–X)_{76}$ amorphous alloys. Acta Metall. 1991;31:925–36.

27. Gutzow I, Dochev V, Pancheva E, Dimov K. Induced crystallization of poly(ethylene terephthalate) on small metallic nucleating particles. J Polym Sci. 1978;16:1155–68.
28. De Fontaine D. Simple models for the omega phase transformation. Metall Trans A. 1988;19:169–75.
29. Sun F, Gloriant T. Primary crystallization process of amorphous $Al_{88}Ni_6Sm_6$ alloy investigated by differential scanning calorimetry and by electrical resistivity. J All Comput. 2009;477:133–8.
30. Prima F, Vermaut P, Texier G, Ansel D, Gloriant T. Evidence of α-nanophase heterogeneous nucleation from ω particles in a β-metastable Ti-based alloy by high-resolution electron microscopy. Scripta Mater. 2006;54:645–8.
31. Sukedai E, Hashimoto H, Tomita M. Investigation of omega-phase in Ti–Mo alloys by high resolution electron microscopy, image processing and dark-field methods. Philos Mag A. 1991;64:1201–8.